

A Spike Learning System for Event-driven Object Recognition

Shibo Zhou^{*1}, Wei Wang^{*2}, Xiaohua Li¹ and Zhanpeng Jin²

¹Binghamton University, State University of New York

{zhou19, xli}@binghamton.edu

²University at Buffalo, State University of New York

{wwang49, zjin}@buffalo.edu

Abstract

Event-driven sensors such as LiDAR and dynamic vision sensor (DVS) have found increased attention in high-resolution and high-speed applications. A lot of work has been conducted to enhance recognition accuracy. However, the essential topic of recognition delay or time efficiency is largely under-explored. In this paper, we present a spiking learning system that uses the spiking neural network (SNN) with a novel temporal coding for accurate and fast object recognition. The proposed temporal coding scheme maps each event's arrival time and data into SNN spike time so that asynchronously-arrived events are processed immediately without delay. The scheme is integrated nicely with the SNN's asynchronous processing capability to enhance time efficiency. A key advantage over existing systems is that the event accumulation time for each recognition task is determined automatically by the system rather than pre-set by the user. The system can finish recognition early without waiting for all the input events. Extensive experiments were conducted over a list of 7 LiDAR and DVS datasets. The results demonstrated that the proposed system had state-of-the-art recognition accuracy while achieving remarkable time efficiency. Recognition delay was shown to reduce by 56.3% to 91.7% in various experiment settings over the popular KITTI dataset.

Keywords: spiking neural network, object recognition, event-driven sensor, LiDAR, DVS, time efficiency.

1 Introduction

Object recognition, as a fundamental and key computer vision (CV) technique, has been substantially investigated over the decades. With the help of deep neural networks (DNNs), great success has been achieved regarding recognition accuracy. However, nearly all of the existing solutions work on digital images or videos that are captured by traditional cameras at a fixed rate, commonly 30 or 60 fps. Such traditional frame-based cameras encounter severe challenges in many

highly demanding applications that require high speed, high accuracy, or high dynamics, such as autonomous driving, unmanned aerial vehicles (UAV), robotics, gesture recognition, etc. [Hwu *et al.*, 2018]. Low frame rate means low temporal resolution and motion blur for high-speed objects. High frame rate leads to a large amount of data with substantial redundancy and a heavy computational burden inappropriate for mobile platforms.

To tackle the above challenges, one of the alternative approaches is event-based sensing [Gallego *et al.*, 2019]. Typical examples include light detection and ranging (LiDAR) sensor, dynamic vision sensor (DVS), and radio detection and ranging (Radar) sensor. LiDAR is a reliable solution for high-speed and precise object detection in a wide view at long distance and has become essential for autonomous driving. DVS cameras have significant advantages over standard cameras with high dynamic range, less motion blur, and extremely small latency [Lichtsteiner *et al.*, 2008].

Traditional cameras capture images or videos in the form of frames. Event-based sensors capture images as asynchronous events. Events are created at different time instances and are recorded or transmitted asynchronously. Each event may have time resolution in the order of microseconds. Because events are sparse, the data amount is kept low even in wide-area 3D spatial sensing or high-speed temporal sensing.

Although some research has been made for object recognition and classification based on event sensors, asynchronous object recognition is mostly still an open objective [Gallego *et al.*, 2019]. Existing methods usually accumulate all the events within a pre-set collection time duration to construct an image frame for recognition. This synchronous processing approach is straight forward and can employ existing DNN methods conveniently. But it overlooks the temporal asynchronous nature of the events and suffers from recognition delays caused by waiting for events accumulation. Too long an accumulation duration leads to image blurring while too short an accumulation duration loses object details. The fixed accumulation duration is a limiting factor to recognition accuracy in practice.

As an example, in [Liu *et al.*, 2016], the DVS sensor had an event rate from 10K to 300K events per second. For fast object tracking, a short fixed accumulation duration of 20 ms was adopted, which resulted in only 200 to 6000 events for each 240×180 image frame. Obviously, this could hardly

*These authors contributed equally to this work.

provide sufficient resolution for the subsequent CNN-based classifier. Novel methods that can recognize objects asynchronously with the accumulation duration optimized according to the nature of object recognition tasks are more desirable.

As another example, a typical 5 Hz LiDAR sensor needs 0.2 seconds to collect all the events for a frame image. During this waiting period, a car travels at 120 km/hour can run near 7 meters. For timely object recognition or accident warning, methods that can process events asynchronously without waiting for the accumulation of the final events are more desirable.

In this paper, we propose a new spike learning system that uses the spiking neural network (SNN) with a novel temporal coding to deal with specifically the task of asynchronous event-driven object recognition. It can reduce recognition delay and realize much better time efficiency. It can maintain competitive recognition accuracy as existing approaches.

Major contributions of this paper are:

- We design a new spike learning system that can exploit both the asynchronous arrival time of events and the asynchronous processing capability of neuron networks to reduce delay and optimize timing efficiency. The first “asynchronous” means that events are processed immediately with a first-come-first-serve mode. The second “asynchronous” means that the network can output recognition results without waiting for all neurons to finish their work. Integrating them together can significantly enhance time efficiency, computational efficiency, and energy efficiency.
- For the first time, recognition time efficiency is defined and evaluated extensively over a list of event-based datasets as one of the major objectives of object recognition.
- We develop a novel temporal coding scheme that converts each event’s asynchronous arrival time and data to SNN spike time. It makes it possible for the learning system to process events immediately without delay and to use the minimum number of events for timely recognition automatically.
- We conduct extensive experiments over a list of 7 event-based datasets such as KITTI [Geiger *et al.*, 2012] and DVS-CIFAR10 [Li *et al.*, 2017]. Experiment results demonstrate that our system had a remarkable time efficiency with competitive recognition accuracy. Over the KITTI dataset, our system reduced recognition delay by 56.3% to 91.7% in various experiment settings.

The rest of the paper is organized as follows. Section 2 introduces the related work. Section 3 provides the details of the proposed spiking learning system. Experiment datasets and results are given in Sections 4 and 5, respectively. We conclude the paper in Section 6.

2 Related Work

LiDAR uses active sensors that emit their own laser pulses for illumination and detects the reflected energy from the objects. Each reflected laser pulse is recorded as an event. From the

events, object detection and recognition can be carried out by various methods, either traditional feature extraction methods or deep learning methods. Behley *et al.* [Behley *et al.*, 2013] proposed a hierarchical segmentation of the laser range data approach to realize object detection. Wang and Posner [Wang and Posner, 2015] applied a voting scheme to process LiDAR range data and reflectance values to enable 3D object detection. Gonzalez *et al.* [González *et al.*, 2017] explored the fusion of RGB and LiDAR-based depth maps. Tatoglu and Pochiraju [Tatoglu and Pochiraju, 2012] presented techniques to model the intensity of the laser reflection during LiDAR scanning to determine the diffusion and specular reflection properties of the scanned surface. Hernandez *et al.* [Hernandez *et al.*, 2014] took advantage of the reflection of the laser beam to identify lane markings on the road surface. Asvadi *et al.* [Asvadi *et al.*, 2017] introduced a convolutional neural network (CNN) to process 3D LiDAR point clouds and predict 2D bounding boxes at the proposal phase. An end-to-end fully convolutional network was used for a 2D point map projected from 3D-LiDAR data in [Li *et al.*, 2016]. Kim and Ghosh [Kim and Ghosh, 2016] proposed a framework utilizing fast R-CNN to improve the detection of regions of interest and the subsequent identification of LiDAR data. Chen *et al.* [Chen *et al.*, 2017] presented a top view projection of the LiDAR point clouds data and performed 3D object detection using a CNN-based fusion network.

DVS, also called neuromorphic vision sensor or silicon retina, records the changing of pixel intensity at fine time resolution as events. DVS-based object recognition is still at an early stage. Lagorce *et al.* [Lagorce *et al.*, 2016] utilized the spatial-temporal information from DVS to build features and proposed a hierarchical architecture for recognition. Liu *et al.* [Liu *et al.*, 2016] combined gray-scale Active Pixel Sensor (APS) images and event frames for object detection. Chen [Chen, 2018] used APS images on a recurrent rolling CNN to produce pseudo-labels and then used them as targets for DVS data to do supervised learning with the tiny YOLO architecture.

Built on the neuromorphic principle, SNN is considered a natural fit for neuromorphic vision sensors and asynchronous event-based sensors. SNN imitates biological neural networks by directly processing spike pulses information with biologically plausible neuronal models [Maass, 1997][Ponulak and Kasinski, 2011]. Regular neural networks process information in a fully synchronized manner, which means every neuron in the network needs to be evaluated. Some SNNs, on the contrary, can work in asynchronous mode, where not all neurons are to be stimulated [Susi *et al.*, 2018]. The attempts of applying SNN for neuromorphic applications include pattern generation and control in neuro-prosthetics systems [Ponulak and Kasinski, 2006], obstacle recognition and avoidance [Ge *et al.*, 2017], spatio- and spectro-temporal brain data mapping [Kasabov, 2014], etc. Attempts were also made to use SNN for object detection and recognition, either over traditional frame-based image data [Cannici *et al.*, 2019; Zhang *et al.*, 2019; Lee *et al.*, 2016], or over event-based LiDAR and DVS data [Zhou *et al.*, 2020][Wu *et al.*, 2019].

A class of SNNs was developed with temporal coding, where spiking time instead of spiking rate or spiking count

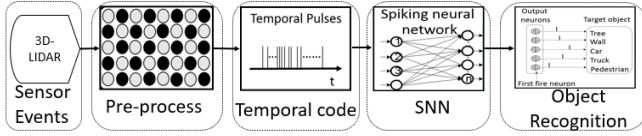


Figure 1: Flow diagram of the proposed spike learning system.

or spiking probability was used to encoding neuron information. The SpikeProp algorithm [Bohte *et al.*, 2002] described the cost function in terms of the difference between desired and actual spike times. It is limited to learning a single spike. Supervised Hebbian learning [Legenstein *et al.*, 2005] and ReSuMe [Ponulak and Kasiński, 2010] were primarily suitable for the training of single-layer networks only.

As far as we know, all the existing SNN works over event-based sensor data need a pre-set time duration to accumulate events into frame-based images before recognition. How to break this limitation to develop SNNs with the full asynchronous operation is still an open problem.

3 A Spike Learning System

Fig. 1 shows the workflow of our proposed spike learning system. The pipeline consists of three major blocks: 1) Pre-processing of asynchronous events from event-based sensors; 2) Temporal coding of the pre-processed events into SNN input spike time; 3) Object recognition with SNN.

3.1 Pre-processing of Events

The event data in standard LiDAR datasets are usually given as tuple (x, y, z, r) , where (x, y, z) is the location of the object, and r is the received light intensity. The events form a point cloud at a certain time-stamp. Existing LiDAR datasets usually contain this time-stamp only instead of event timing. For real-time applications, events may be collected asynchronously. Each event comes with its own arrival time t_a , which is the summation of laser pulse receiving time, LiDAR signal processing time, and data transmission time from the sensor to the learning system.

With voxelization or other similar techniques [Zhou *et al.*, 2020], we can compress the events data by quantizing the large spatial region into a small and fixed 3D integer grid (x_v, y_v, z_v) . For example, many papers quantize the KITTI dataset point cloud into a $768 \times 1024 \times 21$ grid. Let the spatial quantization step sizes in the three dimensions be Δx , Δy , and Δz , respectively. Then the event (x, y, z, r) falls into the voxel

$$\mathcal{V}(x_v, y_v, z_v) = \{(x, y, z) : x_v \Delta x \leq x < (x_v + 1) \Delta x, \\ y_v \Delta y \leq y < (y_v + 1) \Delta y, z_v \Delta z \leq z < (z_v + 1) \Delta z\}. \quad (1)$$

A voxel may have multiple or zero events due to events sparsity. Its value can be set as the number of falling events, light intensity r , object distance $\sqrt{x^2 + y^2 + z^2}$, or laser light flying time $2\sqrt{x^2 + y^2 + z^2}/c$ with light speed c [Zhou *et al.*,

2020]. In our experiments, we set the voxel value as

$$D(x_v, y_v, z_v) = \begin{cases} \frac{2\sqrt{x^2 + y^2 + z^2}}{c}, & (x, y, z) \in \mathcal{V}(x_v, y_v, z_v) \\ 0, & \text{otherwise} \end{cases} \quad (2)$$

We use the first arriving event (x, y, z, r) inside this voxel to calculate $D(x_v, y_v, z_v)$. If no events falling inside this voxel, then $D(x_v, y_v, z_v) = 0$.

For DVS cameras, each event is recorded as (x, y, t, p) , where (x, y) is the pixel coordinate in 2D space, t is the time-stamp or arrival time of the event, and p is the polarity indicating the brightness change over the previous time-stamp. The polarity is usually set as $p(x, y, t) = \pm 1$ or $p(x, y, t) = \{0, 1\}$ [Chen *et al.*, 2019]. Pixels without significant intensity change will not output events. DVS sensors are noisy because of coarse quantization, inherent shot noise in photos, transistor circuit noise, arrival timing jitter, etc.

By accumulating the event stream over an exposure time duration, we can obtain an image frame. Specifically, accumulating events over exposure time from t_0 to t_K gives the image

$$D(x_v, y_v) = \sum_{t=t_0}^{t_K} p(x_v, y_v, t) + I(x_v, y_v), \quad (3)$$

where (x_v, y_v) is the pixel location, and $I(x_v, y_v)$ is the initial image at time t_0 . We can set $I(x_v, y_v) = 0$ from the start. Obviously, longer exposure duration $t_K - t_0$ leads to better image quality for slow-moving objects but blurring for fast-moving objects. Most existing methods pre-set an exposure duration, such as 100 milliseconds for DVS-CIFAR10, to construct the image $D(x_v, y_v)$ for the subsequent recognition. In contrast, our proposed system does not have such a hard exposure time limitation and can automatically give recognition outputs within the best exposure time duration for the tasks.

3.2 Temporal Coding for Spiking Neural Networks

In SNNs, neurons communicate with spikes or action potentials through layers of the network. When a neuron's membrane potential reaches its firing threshold, the neuron will emit a spike and transmit it to other connected neurons [Ponulak and Kasinski, 2011]. We adopt the spike-time-based spiking neuron model of [Mostafa, 2018]. Specifically, we use the non-leaky integrate-and-fire (n-LIF) neuron with exponentially decaying synaptic current kernels. The membrane potential is described by

$$\frac{dv_j(t)}{dt} = \sum_i w_{ji} \kappa(t - t_i), \quad (4)$$

where $v_j(t)$ is the membrane potential of neuron j , w_{ji} is the weight of the synaptic connection from the input neuron i to the neuron j , t_i is the spiking time of the neuron i , and $\kappa(t)$ is the synaptic current kernel function. The value of neuron i is encoded in the spike time t_i . The synaptic current kernel function determines how the spike stimulation decays over time. We use exponential decaying as given below

$$\kappa(t) = u(t)e^{-\frac{t}{\tau}}, \quad (5)$$

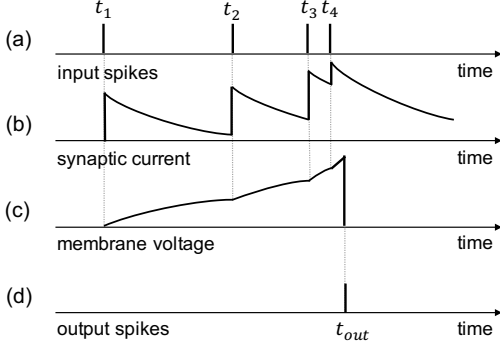


Figure 2: The working principle of the n-LIF neuron model. (a) Four input neurons spike at time t_i , $i = 1, \dots, 4$. (b) Synaptic current $\kappa(t - t_i)$ jumps and decays over time. (c) Membrane voltage potential $v_j(t)$ rises towards the firing threshold. (d) The neuron j emits a spike at time $t_j = t_{out}$ when the threshold is crossed.

where τ is the decaying time constant, and $u(t)$ is the unit step function defined as

$$u(t) = \begin{cases} 1, & \text{if } t \geq 0 \\ 0, & \text{otherwise} \end{cases} \quad (6)$$

Fig. 2 illustrates how this neuron model works. A neuron is only allowed to spike once unless the network is reset or a new input pattern is presented.

An analog circuit to implement this neuron was designed by [Zhou *et al.*, 2020] and was shown to be highly energy efficient. For training or digital (software) implementations, however, we do not need to emulate the operation (4). Instead, we skip the dynamic time-evolution and consider only the member voltage at spiking time t_j . For this purpose, solving (4) we get

$$v_j(t_j) = \sum_{i \in C} w_{ji} \tau \left(1 - e^{-\frac{t_j - t_i}{\tau}}\right), \quad (7)$$

where the set $C = \{i : t_i < t_j\}$ includes all (and only those) input neurons that spike before t_j . Larger τ leads to lower $v_j(t_j)$. For any τ , we can find an appropriate voltage threshold $v_j(t_j)$ so that the activate input neuron set C and the output spike time t_j do not change. Therefore, in digital implementation, we can simply set both the voltage threshold and τ to 1. With $v_j(t_j) = 1$, the neuron j 's spike time satisfies

$$e^{t_j} = \sum_{i \in C} e^{t_i} \frac{w_{ji}}{\sum_{l \in C} w_{jl} - 1}. \quad (8)$$

In software SNN implementation, we can use directly e^{t_i} as neuron value, calculate $w_{ji}/(\sum_{l \in C} w_{jl} - 1)$ as weights, and (8) is then the input-output equation of a feed-forward fully connected neural network layer. We do not need other nonlinear activations because the weights are themselves nonlinear.

At the first (or input) layer, we need to encode the pre-processed event data $D(x_v, y_v, z_v)$ into spike time t_i . Existing methods such as [Zhou *et al.*, 2020] simply let $t_i = D(x_v, y_v, z_v)$, which when applied onto the event-driven data will ignore the inherent temporal information and the

asynchronous property of the events. To fully exploit the asynchronous events property, we propose the following new temporal coding scheme that encodes both event value $D(x_v, y_v, z_v)$ and the arrival time t_a of each event.

Consider a LiDAR event (x, y, z, r) arriving at time t_a . During preprocessing, assume it is used to update the voxel value $D(x_v, y_v, z_v)$. Also assume that this voxel (x_v, y_v, z_v) corresponds to the i th input neuron in the SNN input layer. This neuron's spiking time is then set as

$$t_i = \max\{\beta, t_a\} + \alpha D(x_v, y_v, z_v). \quad (9)$$

where β is a time parameter used to adjust delayed processing of early arrival events, and α is a constant to balance the value of $D(x_v, y_v, z_v)$ and t_a so that the two terms in t_i are not orders-of-magnitude different.

The first term in the right of (9) encodes the event arrival time. If $\beta = 0$, then there is no delay in encoding the arrival time: all the events are processed immediately upon arrival. If β is set to the image frame time, we have the conventional synchronous event processing scheme where object recognition does not start until all the events are accumulated together. We can use β to control the exposure time t_K . The second term encodes the event value. If α is set as 0, then only the event arrival time is encoded. In this case, β should be set as a small value, so that the temporal information could be fully exploited (e.g. if $\beta = 0$, then $t_i = t_a$). As a matter of fact, (9) is a general temporal encoding framework. Various encoding strategies can be realized with appropriate parameters α and β , such as encoding event value only, encoding event arrival time only, and encoding both event value and arrival time.

For DVS sensors, assume similarly that the pixel (x_v, y_v) is the i th input neuron. During the exposure time, while events are being accumulated into $D(x_v, y_v)$ according to (3), the spiking time is set as the smallest t_i that satisfies

$$\sum_{t=t_0}^{t_i} p(x_v, y_v, t) + I(x_v, y_v) \geq \Gamma(t_i). \quad (10)$$

$\Gamma(t)$ is a threshold function that can be set as a constant α or a linear decreasing function

$$\Gamma(t) = \beta(t_K - t), \quad (11)$$

with rate β . If $\beta = 0$, then the neuron spikes immediately when the pixel value is positive. A sufficiently large β effectively makes us wait and accumulate all the events to form a frame image before SNN processing. In this case, we fall back to the traditional synchronous operation mode. If a pixel's intensity accumulates faster, then it spikes earlier. If the pixel accumulates slower or even stays near 0, then it may never spike.

With the proposed temporal coding scheme, the system would be able to output a recognition decision asynchronously after some accumulation time t between t_0 and t_K , and the event accumulation operation stops at t . Only the events during t_0 and t are used for inference. Therefore, t_0 and t_K can be simply set as the start and end time of the recognition task, such as an image frame time. This avoids the headache of looking for the best pre-set accumulation

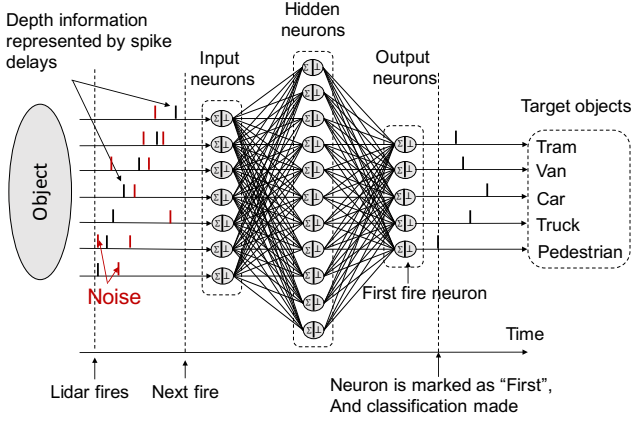


Figure 3: SNN with spiking fully-connected (FC) layers for object recognition.

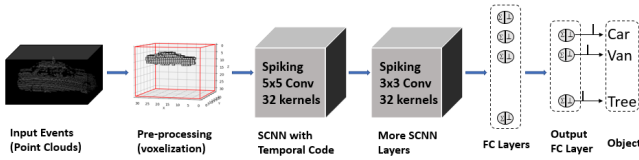


Figure 4: SNN with multiple SCNN layers and FC layers for object recognition.

time. Note that no pre-set accumulation time can be optimal for all images. Some images need longer accumulation, while some other images need short accumulation. The proposed temporal coding enables our system to resolve this challenge in a unique way: We just pre-set a very large accumulation time t_K , and the system can automatically find the optimal accumulation time t used for each image. In other words, instead of the fixed pre-set accumulation time, a unique event accumulation time t (well before t_K) can be found for each image automatically by the system.

3.3 Object recognition with SNN

Many other SNNs use more complex neuron models or use spike counts or rates as neuron values. In comparison, our neuron model is relatively simple and has only a single spike, which makes our SNN easier to train and more energy-efficient when implemented in hardware. Based on the neuron input/output expression (8), the gradient calculation and gradient-descent-based training become nothing different from conventional DNNs.

Based on (8), we can implement both spiking fully-connected (FC) layers and spiking convolutional neural network (SCNN) layers just as conventional DNN FC and CNN layers. Fig. 3 shows an SNN with two FC layers: one input layer with our temporal coding, one hidden FC layer, and one output FC layer. SCNN layers work in a similar way as traditional CNN but are equipped with spiking kernels. For more complex tasks, we can apply multiple SCNN layers and FC layers, as shown in Fig. 4. Pooling layers such as max-pooling and average-pooling can also be used, which is the

same as conventional DNNs. The standard back-propagation technique can be used to train the weights w_{ji} .

For real-time object recognition, the SNN spiking time range is on the same scale as the event arrival time, specifically, starting at t_0 and ending at t_K . The SNN takes in spikes sequentially according to their arrival time. Each neuron keeps accumulating the weighted value and comparing it with the threshold until the accumulation of a set of spikes can fire the neuron. Once the neuron spikes, it would not process any further input spikes unless reset or presented with a new input pattern. The recognition result is made at the time of the first spike among output neurons. Smaller t_j or e^{t_j} means stronger classification output. Also, smaller t_j as output means that inference delay can be reduced, which is an outcome of the asynchronous working principle of SNN.

Define the input of SNN as \mathbf{z}_0 with elements $z_{0,i} = e^{t_i}$, and the output of SNN as \mathbf{z}_L with elements $z_{L,i} = e^{t_{L,i}}$. Then we have $\mathbf{z}_L = f(\mathbf{z}_0; \mathbf{w})$ with nonlinear mapping f and trainable weight \mathbf{w} which includes all SNN weights w_{ji} and the temporal coding parameter β . Let the targeting output be class c , then we train the network with the loss function

$$\mathcal{L}(\mathbf{z}_L, c) = -\ln \frac{z_{L,c}^{-1}}{\sum_{i \neq c} z_{L,i}^{-1}} + k \sum_j \max \left\{ 0, 1 - \sum_i w_{ji} \right\}, \quad (12)$$

where the first term is to make $z_{L,c}$ the smallest (equivalently $t_{L,c}$ the smallest) one, while the second term is to make sure that the sum of input weights of each neuron be larger than 1. The parameter k adjusts the weighting between these two terms.

The training of (12) can be conducted with the standard backpropagation algorithm similar to conventional DNNs, just as [Mostafa, 2018]. Nevertheless, a problem of [Mostafa, 2018] is that its presented algorithm did not require $t_j > t_i$ for $i \in \mathcal{C}$. This led to $t_j \leq t_i$ or even negative t_j that was not practical. We corrected this problem and implemented the training of (12) in the standard deep learning platform TensorFlow.

4 Evaluation Datasets

To investigate the effectiveness of our proposed system, we evaluated it on a list of 7 LiDAR and DVS datasets introduced below. Their sample images are shown in Fig. 5.

4.1 LiDAR Datasets

KITTI Dataset In order to evaluate the ability of our proposed system on complex real-life data in the autonomous driving scenario, we trained and tested it on the KITTI dataset [Geiger *et al.*, 2012]. We utilized the KITTI 3D object detection benchmark, specifically the point clouds data collected by Velodyne HDL-64E rotating 3D laser scanner, which provided 7481 labeled samples. However, the provided point clouds data can not be directly used because all label annotations (location, dimensions, observation angle, etc.) are provided in camera coordinates instead of Velodyne coordinates.

To convert point clouds data onto Velodyne coordinates, we first mapped point clouds data (x, y, z) to an expanded

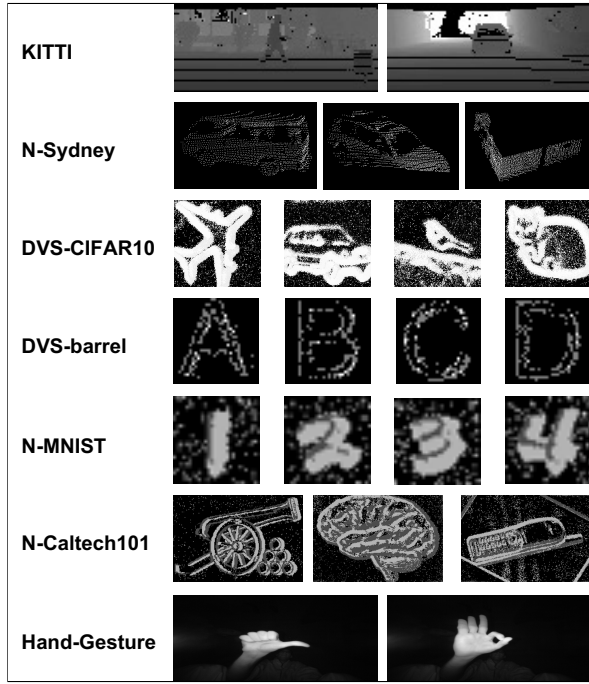


Figure 5: Sample images of LiDAR and DVS datasets used in this paper.

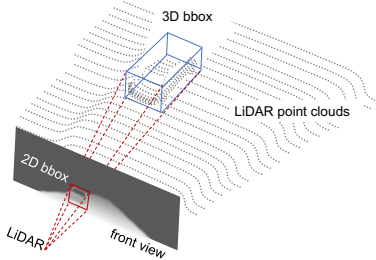


Figure 6: Transformation of KITTI 3D Point Clouds into 2D LiDAR front view images.

front view $(x_{\text{front}}, y_{\text{front}})$, whose size was determined by the resolution of the LiDAR sensor. We used the transformation

$$x_{\text{front}} = \left\lfloor -\frac{\arctan \frac{y}{x}}{R_h} \right\rfloor, y_{\text{front}} = \left\lfloor -\frac{\arctan \frac{z}{\sqrt{x^2+y^2}}}{R_v} \right\rfloor \quad (13)$$

where R_h and R_v are the horizontal and vertical angular resolution in radians, respectively. In order to project the label annotations onto the front view plane, we first calculated the bounding box in camera coordinates and transferred the corners to Velodyne coordinates by multiplying the transition matrix T_{c2v} . The object location was mapped onto the front view similarly, as illustrated in Fig. 6. Based on the front view locations, objects were cropped with a fixed size to establish the recognition dataset.

The changing from 3D to 2D would reduce the computational complexity of recognition. We also artificially gen-

Table 1: Our network models. Sample notation explained: F256 (fully connected layer with 256 spiking neurons), C5-48 (convolutional layer with 48 spiking kernels of size 5×5), AP (average-pooling layer with stride 2).

KITTI	($50 \times 118 \times 1$): C5-48, C5-24, F256, F8
N-Sydney	($32 \times 32 \times 32$): C5-32, C3-32, F128, F9
DVS-barrel	(input 1024): F2000, F36
N-MNIST	($28 \times 28 \times 1$): C5-32, C5-16, F10
N-Caltech101	(200×300): C5-16, C3-8, F64, F101
HandGesture	(120×320): C5-32, C3-48, C3-16, F64, F10
DVS-CIFAR10	Small: C3-32, AP, C3-48, AP, F256, F10
(128×128)	Medium: C3-32, C3-48, AP, C3-64, AP, F256, F10
	Large: C3-32, C3-64, AP, C3-128, C3-256, AP, F1024, F10

erated arrival time t_a for each event (x, y, z) linearly with respect to x . The processed KITTI dataset contains 32456 training samples and 8000 testing samples covering 8 classes of KITTI objects.

N-Sydney The N-Sydney Urban Objects dataset [Chen *et al.*, 2014] is an event-based LiDAR dataset containing 26 object classes. We considered only the following 9 classes: Van, Tree, Building, Car, Truck, 4wd, Bus, Traffic light, and Pillar. We artificially generated arrival time t_a for each event.

4.2 DVS Datasets

DVS-CIFAR10 The DVS-CIFAR10 dataset [Li *et al.*, 2017] is converted from the popular CIFAR10 data set. It has 10000 samples covering 10 classes. We split the dataset into a training set of 8000 samples and a testing set of 2000 samples while adopting the full 128×128 pixel scene.

DVS-barrel The DVS-barrel dataset has 6753 samples with 36 classes [Orchard *et al.*, 2015], which we split into a training set of 3453 samples and a test set of 3000. We used the ‘‘ExtractedStabilized’’ version of the dataset, which, rather than using the full 128×128 pixel scene, extracts individual characters into 32×32 pixel scenes.

N-MNIST, N-Caltech101, Hand-Gesture The N-MNIST [Orchard *et al.*, 2015] and N-Caltech101 [Zhang *et al.*, 2006] datasets are the conversion of two popular image datasets MNIST and Caltech101. The N-MNIST has 10 object classes and image size 28×28 . Caltech101 has 100 object classes plus a background class. The image size on average is 200×300 . The Hand-Gesture dataset [Huang *et al.*, 2011] is a DVS dataset with an image size of 120×320 .

5 Evaluation

5.1 Experiment Setup

Table 1 lists the network configurations we designed based on the proposed spiking learning system architecture for the datasets listed in Fig. 5.

All datasets were tested over models with multiple SCNN and FC layers because our experiments showed that they were much better than simpler SNNs with FC layers only. As for the KITTI dataset, a model with two SCNN layers and two FC layers was employed. The input size was $50 \times 118 \times 1$. The

kernel size for the SCNN layers was 5×5 , with a stride size of 2. The numbers of kernels were 48 and 24, respectively. The output from the second SCNN layer had a size $13 \times 30 \times 24$ and was flattened and passed to the first FC layer (with 256 spiking neurons). The second FC layer had 8 output channels. The batch size was set to 10, and the initial learning rate was $1e-3$ with decay. Adam optimizer was adopted for training.

The N-Sydney Urban Object dataset and the N-Caltech 101 dataset were tested over similar models with two SCNN layers and two FC layers. The Hand-Gesture dataset was tested over a model with three SCNN layers and two FC layers.

The DVS-CIFAR10 dataset was considered the most challenging one among these datasets. It is also much more challenging than the conventional frame-based CIFAR10 due to noisy samples and a single intensity channel. We created three different spiking network structures for a fair comparison with [Wu *et al.*, 2019], which also created three SNN structures to compare with other SNN and DNN results and published the best accuracy so far. The training employed Adam as the optimizer with a batch size of 8, and 100 training epochs with an exponentially decaying learning rate. By manipulating learning rates, the fastest convergence was obtained when the learning rate started at $1e-2$ in epoch 1 and ended at $1e-5$ in epoch 100.

Note that we tried various optimizers such as SGD and Adam on each model during training. Their training performance did not show a significant difference.

5.2 Experiment Results

We used recognition accuracy (A) and recognition (inference) delay (D) as performance metrics to evaluate and compare our models with the state of the arts. Based on A and D we calculated performance gain (G) of our model as

$$G_{\text{acc}} = \frac{A_{\text{ours}} - A_{\text{ref}}}{A_{\text{ref}}}, \quad G_{\text{time}} = \frac{D_{\text{ref}} - D_{\text{ours}}}{D_{\text{ref}}}, \quad (14)$$

where G_{acc} and G_{time} are the accuracy gain and time efficiency gain of our model over some reference model, respectively. The time efficiency gain is also the ratio of delay/latency reduction. The delay includes both the delay of the inference algorithm, which we call ‘‘inference delay’’, and the delay caused by waiting for the asynchronous arrival of events. Their sum is the ‘‘total delay’’. Although we do not directly evaluate computational complex and energy efficiency, we must point out that SNN-based models, in general, have lower computational complexity and higher energy efficiency, as pointed out in [Zhou *et al.*, 2020] and many other SNN publications.

KITTI We take the transformed KITTI dataset as a representative of LiDAR datasets to interpret the evaluation results in detail. The results of other datasets are provided at the end of this section. For the KITTI dataset, we compared our proposed system against the VGG-16 model of conventional CNN. To make the processed KITTI dataset work on VGG-16, we replicated the single intensity channel into three RGB color channels and resized the image from 50×118 to 128×128 . We utilized the VGG-16 pre-trained on ImageNet for transfer learning. Table 2 shows that our system not only

Table 2: Comparison of our SNN model with the VGG-16 model over the KITTI dataset for accuracy and timing efficiency.

Model	VGG-16	Our Model	Gain
Accuracy	91.6%	96.6%	5.46%
Inf. Delay (CPU)	38 ms	8.5 ms	77.6%
Total Delay (CPU)	63 ms	27 ms	57.1%
Inf. Delay (GPU)	23 ms	1.9 ms	91.7%
Total Delay (GPU)	48 ms	21 ms	56.3%

achieved better accuracy (with a gain of $G_{\text{acc}} = 5.46\%$ over VGG-16), but also had much smaller latency or higher time efficiency (with a gain of G_{time} between 56.3% and 91.7% over VGG-16). The reason for VGG-16 to have relatively lower testing accuracy might be because the processed KITTI dataset had a single intensity channel and had a smaller image size than the ideal VGG-16 inputs. A smaller network quite often can achieve better accuracy performance than a complex network over a relatively small dataset.

Next, let us focus on the delay and time efficiency comparison results. To obtain an inference delay, we set temporal coding parameter β for our system to work in synchronous mode, which gave us the SNN’s average running time for an image. We did this over both Intel Core i9 CPU and NVIDIA GeForce RTX 2080Ti GPU. On GPU, our model spent 1.9 ms (millisecond) while VGG-16 needed 23 ms. Our model ran faster because our model both was much simpler and ran asynchronously (inference may terminate at a very small short spiking time t_{out} at the last layer). To obtain the total delay, we set a temporal coding parameter to work in the asynchronous mode to exploit both the asynchronous event arrival property and the SNN’s asynchronous processing property. By contrast, VGG-16 had to wait until all the events were received before starting processing. Since KITTI LiDAR generated 360° image frames at the speed of 10 Hz, the collection of all events for a 90° field-of-view image had a delay of 25 ms. So the total delay on GPU was $25 + 23 = 48$ ms. In contrast, our model had a total delay of 21 ms on average, a delay reduction (and time efficiency gain) of 56.3%. We can also see that the asynchronous events arrival time dominated the total delay. Our model just needed a fraction of events for inference, so it had a much smaller delay.

The distribution of the ratio of events used by our model on the KITTI dataset is shown in Fig. 7(b). On average, 76% of events were used in inference. These figures also demonstrate that our system worked asynchronously and selected automatically various numbers of events in different recognition tasks. In addition, we calculated the ‘‘ideal inference delay’’, which is defined as the difference between the SNN output spike time and the first SNN input spike time. Obviously, ‘‘ideal’’ means that we skip hardware processing delay. The distribution is shown in Fig. 7(a). An interesting observation was that the ‘‘ideal inference time’’ was approximately 1.9 ms, the same as what we obtained from practical GPU running time in Table 2. This may not be surprising because the SNN spiking time duration is usually much longer than GPU executing duration for simple networks. Asynchronous SNN operation can surely reduce recognition/inference delay.

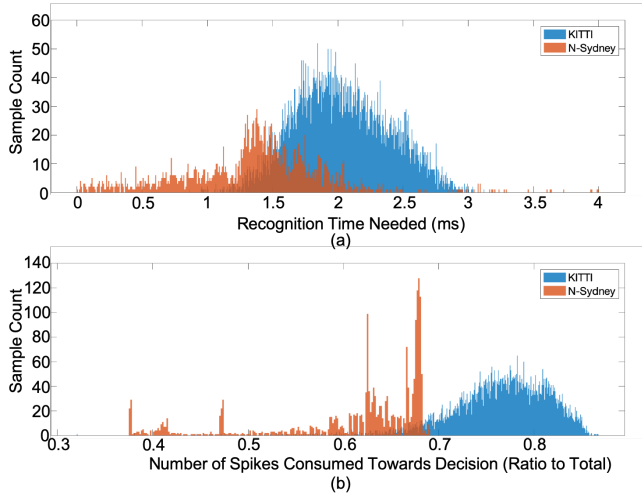


Figure 7: Distributions of (a) inference time and (b) ratio of events used in inference, on LiDAR datasets.

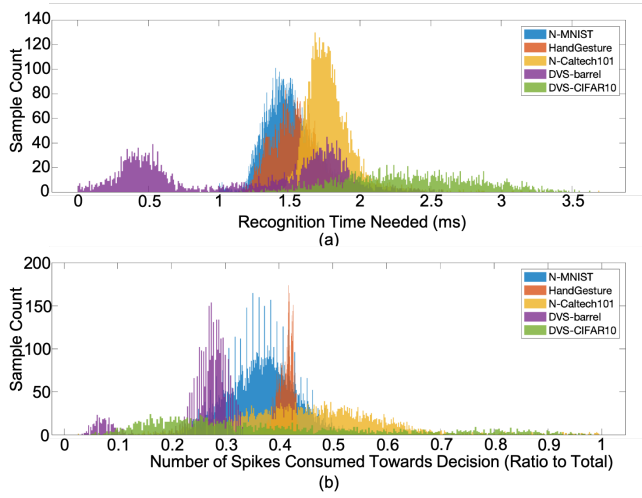


Figure 8: Distributions of (a) inference time and (b) ratio of events used in inference, on DVS datasets.

Based on the above interesting observation, we propose event-ratio as an approximation of time efficiency gain. The event-ratio is defined as the proportion of contributing events (input events consumed before the decision) for recognizing the object in an image frame to all the events corresponding to this image frame, i.e.,

$$r_{\text{event}} = \frac{N_{\text{contributing}}}{N_{\text{all}}}. \quad (15)$$

The estimated time efficiency gain is defined as

$$\hat{G}_{\text{time}} \approx 1 - r_{\text{event}}. \quad (16)$$

The estimation is accurate when the computation delay of CPU and GPU is negligible compared with the event accumulation time duration, which is often true. This way of calculating the time efficiency gain resolves a big hurdle in DVS datasets because DVS datasets usually do not have realistic

Table 3: Summary of accuracy and time efficiency of our system.

Dataset	Accuracy	G_{acc}	Event Ratio	\hat{G}_{time}
KITTI	96.62%	5.46%	0.76	24%
N-Sydney	78.00%	6.85%	0.62	38%
DVS-CIFAR10	69.87%	8.71%	0.38	62%
DVS-Barrel	99.52%	4.32%	0.25	75%
N-MNIST	99.19%	-0.0%	0.37	63%
N-Caltech101	91.89%	-1.6%	0.45	55%
Hand-Gesture	99.99%	0.91%	0.41	59%

Table 4: Comparison with existing results on DVS-CIFAR10

Model	Method	Accuracy
Zhao 2014 [Zhao <i>et al.</i> , 2014]	SNN	22.1%
Lagorce 2016 [Lagorce <i>et al.</i> , 2016]	HOTS	27.1%
Sironi 2018 [Sironi <i>et al.</i> , 2018]	HAT	52.4%
Wu 2019 [Wu <i>et al.</i> , 2019]	SNN	60.5%
Our model (sml)	SCNN	60.8%
Our model (mid)	SCNN	64.3%
Our model (large)	SCNN	69.9%

events timing. Even for LiDAR datasets, event timing could only be constructed artificially. The time efficiency gain (16) catches the key factor, i.e., asynchronous operation, and skips the variations caused by non-ideal software coding and platforms.

Adopting this approximation, the accuracy and time efficiency of our models on all the datasets are listed in Table 3. Gain G_{acc} was calculated by choosing the accuracy of the best model used in our comparison as G_{ref} , see Table 4 and Table 5. From the table, we can see that our system, in general, was competitive with the state-of-the-art models in recognition accuracy. More importantly, our system needed only a fraction of the events, which lead to a 34% to 75% gain in time efficiency.

DVS-CIFAR10 We take DVS-CIFAR10 as an example to detail the evaluations on DVS datasets. The results of all other DVS datasets are given at the end of this section. Table 4 shows that our model had 69.87% recognition accuracy, higher than competitive models listed. Note that the competitive models were selected carefully according to their importance for the development of this dataset and their state-of-art performance. Their accuracy values were cited directly from the papers. Their methods were also listed to show clearly the performance difference of conventional machine learning methods, DNN/CNN, and SNN/SCNN. The reduction of the delay was even more striking based on the description of Table 3. From Fig. 8(b), we can see that our model used only 38% of events for inference, which means a delay reduction of over 62%. From Fig. 8(a), our model on average used 2.35 ms for inference based on our artificially created timing information of the events similar to KITTI.

The effect of different network configurations on the training process was investigated and depicted in Fig. 9, where the training loss was calculated with 8 images randomly sampled from the training set. When being trained on the DVS-

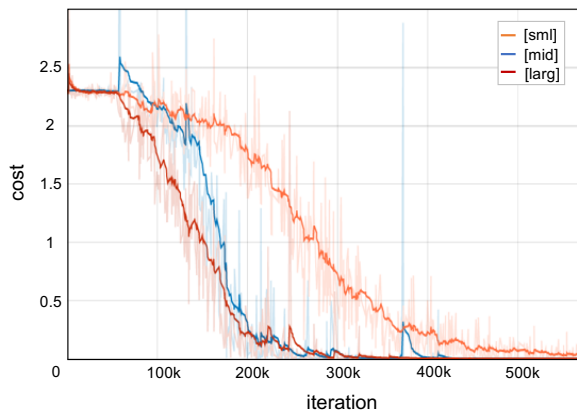


Figure 9: Training convergence of the proposed models over the DVS-CIFAR10 dataset.

CIFAR10 dataset, the larger model converged faster than the smaller one, which might be because of the better capability of larger SNN in learning data representations.

Other datasets For the rest of the datasets, N-Sydney, DVS-barrel, N-MNIST, N-Caltech101, and Hand-Gesture, the accuracy comparisons with the state-of-the-art models are listed in Table 5. The table also listed the major network architecture. We can see that our models provided competitive recognition accuracy. For challenging datasets with relatively lower recognition accuracy, such as N-Sydney, our model had much higher performance. For the popular N-MNIST dataset, our model had relatively low computational complexity because the number of trainable weights ($2.2e4$) was lower than other models.

The event-ratio/inference-time distributions of our SNN model on LiDAR and DVS datasets are shown respectively in Fig. 7 and Fig. 8. On average, 62% of events were needed for the N-Sydney dataset, while the DVS datasets mostly took less than 50% of events to accomplish the inference. It can also be seen that the inference time for most samples was in the range of 1 to 3 ms, demonstrating a strong performance in time efficiency.

6 Conclusion and Future Work

In this paper, we proposed a spiking learning system utilizing temporal-coded spike neural networks for efficient object recognition from event-based sensors such as LiDAR and DVS. A novel temporal coding scheme was developed, which permits the system to exploit the asynchronously arrived sensor events without delay. Integrating nicely with the asynchronous processing nature of SNN, the system can achieve superior timing efficiency. The performance of the system was evaluated on a list of 7 LiDAR and DVS datasets. The experiment proved that the proposed method achieved remarkable accuracy on real-world data and significantly reduced recognition delay. This paper demonstrates the potential of SNN in challenging applications involving high speed and dynamics.

On the other hand, although we developed the general tem-

poral encoding scheme in Section 3.2, the hyper-parameters of the encoding rules (9) (10) were not optimized in our experiments. But rather, we used some hand-picked parameter values heuristically. Thanks to the cost function (12), the training of SNN led to the minimum spike timing $t_{L,i}$ in the final output layer, which means that we still obtained a self-optimized event accumulation time t . It will be an interesting future research topic to optimize directly these hyper-parameters by either including them into the cost function (12) or using the genetic algorithm. This will optimize the event accumulation time t to further enhance recognition accuracy and reduce recognition delay. In addition, we evaluated our learning system for single-object recognition or classification in every single image only. It remains to extend this system to object detection and/or continuous video processing, which will make the study of time efficiency more interesting. Considering the small size of the event-driven datasets used in this paper, only relatively simple SNNs were applied because there would be over-fitting otherwise. This might be one of the reasons for our SNN model’s surprisingly better performance than VGG-16 shown in Table 2. It will be an interesting work to adapt our system to large event-based datasets in the future.

Table 5: Performance comparison over N-Sydney, N-MNIST, N-Caltech101 and Hand-Gesture datasets.

Dataset	Model	Accuracy	Method
N-Sydney	Chen'14 [Chen <i>et al.</i> , 2014]	71%	GFH+SVM
	Maturana'15 [Maturana and Scherer, 2015]	73%	CNN
	Our Model	78%	SCNN
DVS-Barrel	Perez'13 [Pérez-Carrasco <i>et al.</i> , 2013]	95.2%	CNN
	Perez'13 [Pérez-Carrasco <i>et al.</i> , 2013]	91.6%	SCNN
	Orchard'15 [Orchard <i>et al.</i> , 2015]	84.9%	HFirst
	Our Model	99.5%	SCNN
N-MNIST	Orchard'15 [Orchard <i>et al.</i> , 2015]	71.20%	HFirst, 1.2e5
	Neil'16 [Neil <i>et al.</i> , 2016]	97.30%	LSTM, 4.5e4
	Lee'16 [Lee <i>et al.</i> , 2016]	98.70%	SNN, 1.8e6
	Shreshtha'18 [Shreshtha and Orchard, 2018]	99.20%	SNN, 7.2e4
	Wu'18 [Wu <i>et al.</i> , 2018]	98.78%	SNN, 1.8e6
	Our Model	99.15%	SCNN, 2.2e4
N-Caltech101	Zhang'06 [Zhang <i>et al.</i> , 2006]	66.23%	SVM-KNN
	Donahue'14 [Donahue <i>et al.</i> , 2014]	86.91%	DNN
	Chatfield'14 [Chatfield <i>et al.</i> , 2014]	88.54%	CNN
	He'15 [He <i>et al.</i> , 2015]	93.42%	CNN
	Orchard'15 [Orchard <i>et al.</i> , 2015]	5.4%	HFirst, SNN
	Sironi'18 [Sironi <i>et al.</i> , 2018]	64.2%	HATS, SNN
Our Model	91.9%	SCNN	
Hand-Gesture	Huang'11 [Huang <i>et al.</i> , 2011]	94%	GF
	Mantecon'16 [Mantecón <i>et al.</i> , 2016]	99%	SVM
	Our Model	99.9%	SCNN

References

- [Asvadi *et al.*, 2017] Alireza Asvadi, Luis Garrote, Cristiano Prevedida, Paulo Peixoto, and Urbano J Nunes. DepthCN: Vehicle detection using 3D-LIDAR and ConvNet. In *IEEE 20th International Conference on Intelligent Transportation Systems*, pages 1–6. IEEE, 2017.
- [Behley *et al.*, 2013] Jens Behley, Volker Steinhage, and Armin B Cremers. Laser-based segment classification using a mixture of bag-of-words. In *IEEE/RSJ International Conference on Intelligent Robots and Systems (IROS)*, pages 4195–4200. IEEE, 2013.
- [Bohte *et al.*, 2002] Sander M Bohte, Joost N Kok, and Han La Poutre. Error-backpropagation in temporally encoded networks of spiking neurons. *Neurocomputing*, 48(1-4):17–37, 2002.
- [Cannici *et al.*, 2019] Marco Cannici, Marco Ciccone, Andrea Romanoni, and Matteo Matteucci. Asynchronous convolutional networks for object detection in neuromorphic cameras. In *Proceedings of the IEEE Conference on Computer Vision and Pattern Recognition Workshops*, pages 0–0, 2019.
- [Chatfield *et al.*, 2014] Ken Chatfield, Karen Simonyan, Andrea Vedaldi, and Andrew Zisserman. Return of the devil in the details: Delving deep into convolutional nets. *arXiv preprint arXiv:1405.3531*, 2014.
- [Chen *et al.*, 2014] Tongtong Chen, Bin Dai, Daxue Liu, and Jinze Song. Performance of global descriptors for velodyne-based urban object recognition. In *2014 IEEE Intelligent Vehicles Symposium Proceedings*, pages 667–673. IEEE, 2014.
- [Chen *et al.*, 2017] Xiaozhi Chen, Huimin Ma, Ji Wan, Bo Li, and Tian Xia. Multi-view 3D object detection network for autonomous driving. In *IEEE CVPR*, volume 1, page 3, 2017.
- [Chen *et al.*, 2019] Guang Chen, Hu Cao, Canbo Ye, Zhenyan Zhang, Xingbo Liu, Xuhui Mo, Zhongnan Qu, Jorg Conradt, Florian Rohrbein, and Alois C Knoll. Multi-cue event information fusion for pedestrian detection with neuromorphic vision sensors. *Frontiers in Neurobotics*, 13:10, 2019.
- [Chen, 2018] Nicholas FY Chen. Pseudo-labels for supervised learning on dynamic vision sensor data, applied to object detection under ego-motion. In *Proceedings of the IEEE Conference on Computer Vision and Pattern Recognition Workshops*, pages 644–653, 2018.
- [Donahue *et al.*, 2014] Jeff Donahue, Yangqing Jia, Oriol Vinyals, Judy Hoffman, Ning Zhang, Eric Tzeng, and Trevor Darrell. Decaf: A deep convolutional activation feature for generic visual recognition. In *International Conference on Machine Learning*, pages 647–655, 2014.
- [Gallego *et al.*, 2019] Guillermo Gallego, Tobi Delbruck, Garrick Orchard, Chiara Bartolozzi, Brian Taba, Andrea Censi, Stefan Leutenegger, Andrew Davison, Joerg Conradt, Kostas Daniilidis, et al. Event-based vision: A survey. *arXiv preprint arXiv:1904.08405*, 2019.

- [Ge *et al.*, 2017] Chenjie Ge, Nikola Kasabov, Zhi Liu, and Jie Yang. A spiking neural network model for obstacle avoidance in simulated prosthetic vision. *Information Sciences*, 399:30–42, 2017.
- [Geiger *et al.*, 2012] Andreas Geiger, Philip Lenz, and Raquel Urtasun. Are we ready for autonomous driving? the KITTI vision benchmark suite. In *IEEE Conference on Computer Vision and Pattern Recognition (CVPR)*, pages 3354–3361, 2012.
- [González *et al.*, 2017] Alejandro González, David Vázquez, Antonio M López, and Jaume Amores. On-board object detection: Multicue, multimodal, and multiview random forest of local experts. *IEEE Transactions on Cybernetics*, 47(11):3980–3990, 2017.
- [He *et al.*, 2015] Kaiming He, Xiangyu Zhang, Shaoqing Ren, and Jian Sun. Spatial pyramid pooling in deep convolutional networks for visual recognition. *IEEE Transactions on Pattern Analysis and Machine Intelligence*, 37(9):1904–1916, 2015.
- [Hernandez *et al.*, 2014] Danilo Caceres Hernandez, Van-Dung Hoang, and Kang-Hyun Jo. Lane surface identification based on reflectance using laser range finder. In *IEEE/SICE International Symposium on System Integration (SII)*, pages 621–625. IEEE, 2014.
- [Huang *et al.*, 2011] Deng-Yuan Huang, Wu-Chih Hu, and Sung-Hsiang Chang. Gabor filter-based hand-pose angle estimation for hand gesture recognition under varying illumination. *Expert Systems with Applications*, 38(5):6031–6042, 2011.
- [Hwu *et al.*, 2018] Tiffany Hwu, Alexander Y Wang, Nicolas Oros, and Jeffrey L Krichmar. Adaptive robot path planning using a spiking neuron algorithm with axonal delays. *IEEE Transactions on Cognitive and Developmental Systems*, 10(2):126–137, 2018.
- [Kasabov, 2014] Nikola K Kasabov. NeuCube: A spiking neural network architecture for mapping, learning and understanding of spatio-temporal brain data. *Neural Networks*, 52:62–76, 2014.
- [Kim and Ghosh, 2016] Taewan Kim and Joydeep Ghosh. Robust detection of non-motorized road users using deep learning on optical and LIDAR data. In *IEEE 19th International Conference on Intelligent Transportation Systems (ITSC)*, pages 271–276. IEEE, 2016.
- [Lagorce *et al.*, 2016] Xavier Lagorce, Garrick Orchard, Francesco Galluppi, Bertram E Shi, and Ryad B Benosman. Hots: a hierarchy of event-based time-surfaces for pattern recognition. *IEEE Transactions on Pattern Analysis and Machine Intelligence*, 39(7):1346–1359, 2016.
- [Lee *et al.*, 2016] Jun Haeng Lee, Tobi Delbruck, and Michael Pfeiffer. Training deep spiking neural networks using backpropagation. *Frontiers in Neuroscience*, 10:508, 2016.
- [Legenstein *et al.*, 2005] Robert Legenstein, Christian Naeger, and Wolfgang Maass. What can a neuron learn with spike-timing-dependent plasticity? *Neural Computation*, 17(11):2337–2382, 2005.
- [Li *et al.*, 2016] Bo Li, Tianlei Zhang, and Tian Xia. Vehicle detection from 3D LiDAR using fully convolutional network. *arXiv preprint arXiv:1608.07916*, 2016.
- [Li *et al.*, 2017] Hongmin Li, Hanchao Liu, Xiangyang Ji, Guoqi Li, and Luping Shi. CIFAR10-DVS: An event-stream dataset for object classification. *Frontiers in neuroscience*, 11:309, 2017.
- [Lichtsteiner *et al.*, 2008] Patrick Lichtsteiner, Christoph Posch, and Tobi Delbruck. A 128×128 120 db 15μ s latency asynchronous temporal contrast vision sensor. *IEEE Journal of Solid-State Circuits*, 43(2):566–576, 2008.
- [Liu *et al.*, 2016] Hongjie Liu, Diederik Paul Moeys, Gautham Das, Daniel Neil, Shih-Chii Liu, and Tobi Delbrück. Combined frame-and event-based detection and tracking. In *2016 IEEE International Symposium on Circuits and Systems (ISCAS)*, pages 2511–2514. IEEE, 2016.
- [Maass, 1997] Wolfgang Maass. Networks of spiking neurons: the third generation of neural network models. *Neural networks*, 10(9):1659–1671, 1997.
- [Mantecón *et al.*, 2016] Tomás Mantecón, Carlos R del Blanco, Fernando Jaureguizar, and Narciso García. Hand gesture recognition using infrared imagery provided by leap motion controller. In *International Conference on Advanced Concepts for Intelligent Vision Systems*, pages 47–57. Springer, 2016.
- [Maturana and Scherer, 2015] Daniel Maturana and Sebastian Scherer. Voxnet: A 3d convolutional neural network for real-time object recognition. In *IEEE/RSJ International Conference on Intelligent Robots and Systems (IROS)*, pages 922–928. IEEE, 2015.
- [Mostafa, 2018] Hesham Mostafa. Supervised learning based on temporal coding in spiking neural networks. *IEEE Transactions on Neural Networks and Learning Systems*, 29(7):3227–3235, 2018.
- [Neil *et al.*, 2016] Daniel Neil, Michael Pfeiffer, and Shih-Chii Liu. Phased LSTM: Accelerating recurrent network training for long or event-based sequences. In *Advances in Neural Information Processing Systems*, pages 3882–3890, 2016.
- [Orchard *et al.*, 2015] Garrick Orchard, Cedric Meyer, Ralph Etienne-Cummings, Christoph Posch, Nitish Thakor, and Ryad Benosman. HFirst: a temporal approach to object recognition. *IEEE Transactions on Pattern Analysis and Machine Intelligence*, 37(10):2028–2040, 2015.
- [Pérez-Carrasco *et al.*, 2013] José Antonio Pérez-Carrasco, Bo Zhao, Carmen Serrano, Begona Acha, Teresa Serrano-Gotarredona, Shouchun Chen, and Bernabé Linares-Barranco. Mapping from frame-driven to frame-free event-driven vision systems by low-rate rate coding and coincidence processing—application to feedforward ConvNets. *IEEE Transactions on Pattern Analysis and Machine Intelligence*, 35(11):2706–2719, 2013.
- [Ponulak and Kasinski, 2006] Filip Ponulak and Andrzej Kasinski. ReSuMe learning method for spiking neural net-

- works dedicated to neuroprostheses control. In *Proceedings of EPFL LATSIS Symposium 2006, Dynamical Principles for Neuroscience and Intelligent Biomimetic Devices*, pages 119–120. Citeseer, 2006.
- [Ponulak and Kasiński, 2010] Filip Ponulak and Andrzej Kasiński. Supervised learning in spiking neural networks with ReSuMe: sequence learning, classification, and spike shifting. *Neural Computation*, 22(2):467–510, 2010.
- [Ponulak and Kasinski, 2011] Filip Ponulak and Andrzej Kasinski. Introduction to spiking neural networks: Information processing, learning and applications. *Acta Neurobiologiae Experimentalis*, 71(4):409–433, 2011.
- [Shrestha and Orchard, 2018] Sumit Bam Shrestha and Garrick Orchard. Slayer: Spike layer error reassignment in time. In *Advances in Neural Information Processing Systems*, pages 1412–1421, 2018.
- [Sironi *et al.*, 2018] Amos Sironi, Manuele Brambilla, Nicolas Bourdis, Xavier Lagorce, and Ryad Benosman. HATS: Histograms of averaged time surfaces for robust event-based object classification. In *Proceedings of the IEEE Conference on Computer Vision and Pattern Recognition*, pages 1731–1740, 2018.
- [Susi *et al.*, 2018] Gianluca Susi, Pilar Garces, Alessandro Cristini, Emanuele Paracone, Mario Salerno, Fernando Maestu, and Ernesto Pereda. FNS: an event-driven spiking neural network framework for efficient simulations of large-scale brain models. *arXiv preprint arXiv:1801.00864*, 2018.
- [Tatoglu and Pochiraju, 2012] Akin Tatoglu and Kishore Pochiraju. Point cloud segmentation with LIDAR reflection intensity behavior. In *IEEE International Conference on Robotics and Automation (ICRA)*, pages 786–790, 2012.
- [Wang and Posner, 2015] Dominic Zeng Wang and Ingmar Posner. Voting for voting in online point cloud object detection. *Robotics: Science and Systems*, 1(3), 2015.
- [Wu *et al.*, 2018] Yujie Wu, Lei Deng, Guoqi Li, Jun Zhu, and Luping Shi. Spatio-temporal backpropagation for training high-performance spiking neural networks. *Frontiers in Neuroscience*, 12:331, 2018.
- [Wu *et al.*, 2019] Yujie Wu, Lei Deng, Guoqi Li, Jun Zhu, Yuan Xie, and Luping Shi. Direct training for spiking neural networks: Faster, larger, better. In *Proceedings of the AAAI Conference on Artificial Intelligence*, volume 33, pages 1311–1318, 2019.
- [Zhang *et al.*, 2006] Hao Zhang, Alexander C Berg, Michael Maire, and Jitendra Malik. SVM-KNN: Discriminative nearest neighbor classification for visual category recognition. In *IEEE Computer Society Conference on Computer Vision and Pattern Recognition (CVPR’06)*, volume 2, pages 2126–2136. IEEE, 2006.
- [Zhang *et al.*, 2019] Lei Zhang, Shengyuan Zhou, Tian Zhi, Zidong Du, and Yunji Chen. TDSNN: From deep neural networks to deep spike neural networks with temporal coding. In *Proceedings of the AAAI Conference on Artificial Intelligence*, volume 33, pages 1319–1326, 2019.
- [Zhao *et al.*, 2014] Bo Zhao, Ruoxi Ding, Shoushun Chen, Bernabe Linares-Barranco, and Huajin Tang. Feedforward categorization on AER motion events using cortex-like features in a spiking neural network. *IEEE Transactions on Neural Networks and Learning Systems*, 26(9):1963–1978, 2014.
- [Zhou *et al.*, 2020] Shibo Zhou, Ying Chen, Xiaohua Li, and Arindam Sanya. Deep SCNN-based real-time object detection for self-driving vehicles using LiDAR temporal data. *IEEE Access*, 8:76903–76912, 2020.